The Astrophysical Journal, 817:107 (14pp), 2016 February 1 doi:10.3847/0004-637X/817/2/107

ATMOSPHERES OF LOW-MASS PLANETS: THE "BOIL-OFF"

James E. Owen[1,3] and Yanqin Wu[2]
[1] Institute for Advanced Study, Einstein Drive, Princeton NJ, 08540, USA; jowen@ias.edu
[2] Department of Astronomy and Astrophysics, University of Toronto, Toronto, ON M5S 3H4, Canada
Received 2015 June 3; accepted 2015 December 11; published 2016 January 26

ABSTRACT

We show that, for a low-mass planet that orbits its host star within a few tenths of an AU (like the majority of the *Kepler* planets), the atmosphere it was able to accumulate while embedded in the protoplanetary disk may not survive unscathed after the disk disperses. This gas envelope, if more massive than a few percent of the core (with a mass below $10M_{\oplus}$), has a cooling time that is much longer than the timescale on which the planet exits the disk. As such, it could not have contracted significantly from its original size, of the order of the Bondi radius. So a newly exposed protoplanet would be losing mass via a Parker wind that is catalyzed by the stellar continuum radiation. This represents an intermediate stage of mass-loss, occurring soon after the disk has dispersed, but before the EUV/X-ray driven photoevaporation becomes relevant. The surface mass-loss induces a mass movement within the envelope that advects internal heat outward. As a result, the planet atmosphere rapidly cools down and contracts, until it has reached a radius of the order of 0.1 Bondi radius, at which time the mass-loss effectively shuts down. Within a million years after the disk disperses, we find a planet that has only about 10% of its original envelope, and a Kelvin–Helmholtz time that is much longer than its actual age. We suggest that this "boil-off" process may be partially responsible for the lack of planets above a radius of $2.5R_{\oplus}$ in the *Kepler* data, provided planet formation results in initial envelope masses of tens of percent.

Key words: planet–disk interactions – planets and satellites: composition – planets and satellites: formation – protoplanetary disks

1. INTRODUCTION

The *Kepler* observatory has revealed the presence of a large number of close-in ($\lesssim$1 AU), small ($\lesssim 4R_{\oplus}$) (Borucki et al. 2011; Batalha et al. 2013; Mullally et al. 2015), and low-mass ($\lesssim 20M_{\oplus}$) exoplanets (Dumusque et al. 2014; Marcy et al. 2014; Dressing et al. 2015). In fact this type of planet is so frequent that most stars are thought to contain one (e.g., Fressin et al. 2013; Petigura et al. 2013; Silburt et al. 2015). We nickname these planets "*Kepler* planets." They may represent the dominant mode of planet formation, allowing us to calibrate our planet formation models and finally understand this illusive problem.

Unlike the terrestrial planets in our own solar system, the inferred masses and radii of the *Kepler* planets indicate that a large fraction contain H/He rich envelopes (Wu & Lithwick 2013; Hadden & Lithwick 2014; Rogers 2014; Weiss & Marcy 2014). Even among ones that appear to be naked cores, it has been argued that hydrodynamical escape may have occurred and removed their primordial envelopes (Lopez & Fortney 2013; Owen & Wu 2013). This indicates that, in most cases, planet assembly must have finished by the time gas-rich protoplanetary disks disperse after a few Myr.

The size distribution of *Kepler* planets exhibits a puzzling feature: there appears to be a concentration of planets with sizes $\sim 2.5R_{\oplus}$, with a steep fall-off in number at larger sizes, and a possible reduction in number toward smaller sizes (Petigura et al. 2013; Foreman-Mackey et al. 2014; Silburt et al. 2015), although the quantitative details are still uncertain. For the mass range of interest, a size of $2.5R_{\oplus}$ corresponds to an envelope mass fraction of $\sim$1% (Wu & Lithwick 2013; Wolfgang & Lopez 2015). Why does nature favor such an envelope mass, when the environments (e.g., gas density, temperature) for planet formation may be highly diverse and time varying?

There are currently two schools of thought for where these planets formed: either they are formed "in situ," close to their current small orbital separations (e.g., Hansen & Murray 2012; Chiang & Laughlin 2013), or they formed at larger separations and were then migrated to current positions (e.g., Ida & Lin 2005, 2010; Bodenheimer & Lissauer 2014; Raymond & Cossou 2014). Even in the latter scenario, the final planet assembly and the gas accretion may have occurred near the host stars. *Kepler* planets that are in high multiple systems appear to be so closely packed (e.g., the Kepler-11 system, Lissauer et al. 2011; Mahajan & Wu 2014) that they would have been skirting dynamical instabilities in the final assembly had they not been subject to substantial eccentricity dissipation (Pu & Wu 2015). Their current low values of eccentricities (Wu & Lithwick 2013; Hadden & Lithwick 2014) also attest to this dissipation. Gas is the most obvious source of this damping.

Could the gas accretion process, at a distance of $\sim$0.1 AU from the host star, naturally give rise to the above-mentioned 1% envelope mass? The answer is no, at least not according to current theories. In the theory of core-accretion (e.g., Pollack et al. 1996), a planetary embryo embedded in a gas disk will quickly acquire a hydrostatic envelope extending out to its Bondi sphere[4], with a radius[5]

$$R_B = \frac{GM_p}{2c_s^2}, \tag{1}$$

[3] Hubble Fellow.

[4] In the inner disk, the Bondi radius is smaller than the Hill Sphere for the core masses we are concerned about (e.g., Rafikov 2006).

[5] It is yet unclear exactly where the protoplanet's envelope ends and where the disk begins. Background shear in the disk can affect the transition radius (Lissauer et al. 2009), as can 3D flow dynamics (Fung et al. 2015; Ormel et al. 2015). We ignore these complications here.

where M_p is the protoplanet's mass and c_s is the isothermal sound speed of the surrounding gas. The atmosphere, confined by an external disk pressure, has a mass that is roughly the background gas density times the volume of the Bondi sphere (Rafikov 2006). If this is the final atmosphere that we observe, its mass should depend on gas density, temperature, and embryo mass. The observed clustering around 1% mass fraction therefore comes as a surprise.

Multiple works have suggested that the above mass estimates may not be the final envelope mass. Ikoma & Hori (2012) argued that, as the gas disk gradually dissipates away, lifting of the pressure confinement will slowly erode away the envelope. In contrast, Lee et al. (2014) asserted that due to a lack of planetesimal bombardment and associated heating for embryos in the inner disk, the above mentioned hydrostatic envelope will cool and contract, allowing the embryo to accrete ever more gas. In fact, they found that even a $5M_\oplus$ planet may accrete so much gas as to undergo unstable runaway growth (Mizuno et al. 1978). We return to comment on these works later in the discussion. Instead, in this work, we focus on a different aspect of the problem, namely, the case where the nascent disk disappears quickly (as indicated observationally, e.g., Koepferl et al. 2013), leaving the newly formed planet exposed to stellar irradiation and a vacuum boundary condition. We argue that this brings about vigorous mass-loss and rapid cooling, strongly impacting the final envelope mass. This process, happening in the final stage of low-mass planet formation, may potentially help explain the 1% convergence one observes in *Kepler planets*.

This new stage of mass-loss is distinctively different from the process discribed in Ikoma & Hori (2012) and from the mass-loss induced by EUV/X-ray photoevaporation (Lopez & Fortney 2013; Owen & Wu 2013). As our calculations show (Section 3), it occurs because the planet is highly inflated and because it is strongly illuminated by stellar photons. Both these conditions may be satisfied for low-mass planets that newly emerge out of the protoplanetary disk, due to their long thermal timescales (Section 2). The mass-loss takes the form of a Parker wind (Parker 1958) that is heated by continuum stellar radiation (as opposed to only high energy photons). But the ultimate energy source is the internal heat of the planet. As a result of envelope removal, the planet cools and contracts quickly (Section 4). We consider the implications of this work in Section 4 and conclude in Section 5.

In this work we concentrate purely on the case of a rocky core surrounded by a H/He envelope, i.e., the structure most likely to arise from planets forming close to their star in a gaseous disk, although we note that many other structures are still consistent with the observed planet population (e.g., Rogers & Seager 2010).

2. INITIAL CONDITIONS AND PRESENCE OF MASS-LOSS

Planets can lose their atmospheres over time. This process is more extreme when the planets are strongly irradiated and highly inflated. We argue here that this may be just the thermal state the *Kepler* planets found themselves in, when their parent disks dissipated. The process we are interested in occurs within 10^4–10^5 years after the disk dispersal, before the EUV/X-ray photoevaporation has had much of an effect. The latter occurs on a timescale of 10^8 years (Owen & Wu 2013).

2.1. A Wind is Driven

The blackbody temperature at a distance a from a star with surface temperature T_* and radius R_* is

$$T_{\rm eq} = 886\ {\rm K}\left(\frac{T_*}{5800\ {\rm K}}\right)\left(\frac{R_*}{1\ R_\odot}\right)^{1/2}\left(\frac{a}{0.1\ {\rm AU}}\right)^{-1/2}. \quad (2)$$

This is also the photospheric temperature of a planet when its internal luminosity is subordinate to stellar irradiation and when it is exposed to direct sunlight. In this paper, we assume that the gas above the photosphere, in particular, the extended atmosphere that is the outflow we are investigating, will also be heated to roughly this temperature. This could happen due to the absorption of continuum photons by the dust grains embedded in the outflow, when they are present, or by absorption of ionizing photons by the gas molecules when dust is absent. The planet distances of concern lie beyond the dust sublimation radius. So we expect dust formation to be efficient in the outflow. In this work, we do not attempt to model the temperature profile in the extended atmosphere, a shortcoming we hope to remedy in future works. We do remark that the condition of isothermal wind sets an upper bound to the mass-loss rate: the energy advected by the wind should not exceed stellar energy deposit in the wind, or else the isothermal condition will break.

An isothermal atmosphere has an outwardly increasing scale height and can only be in hydrostatic equilibrium if the ambient pressure is sufficiently strong to confine it. This confining pressure was provided by the protoplanetary disk while it was around, but once it dissipated, the only candidate is the stellar wind, which, even at the phenomenal mass-loss rate of young stars (e.g., Wood et al. 2002), falls far too short to be of use. So the isothermal atmosphere is not hydrostatic but instead harbors a so-called "Parker wind" (Parker 1958), with a sonic radius at

$$R_s = \frac{GM_p}{2c_s^2} = R_B. \quad (3)$$

Note the fact that the sonic radius and the Bondi radius are identical is not accidental, but represents the symmetry between outflow and accretion.

Energetically speaking, the stellar continuum radiation, which maintains the isothermality of the wind, is the reason for the mass-loss. However, as we will discover, the mass-loss brings about a rapid gravitational contraction of the planet. The binding energy released during this contraction fuels the mass-loss. There are thus two energy sources for the mass-loss, with the bottom (planet interior) pushing material up, and the top (stellar heating) pulls the material further away from the planet.

2.2. Race between Cooling and Dispersal

The importance of our new mechanism depends critically on the size of the planet when it was first exposed to direct stellar irradiation. A highly inflated planet, with the photosphere at its

Bondi radius, will experience a remarkable mass-loss rate of

$$\dot{M}_p \sim 4\pi R_B^2 \rho_{\rm surf} c_s = 4\pi R_B^2 \frac{P_{\rm surf}}{c_s}$$
$$\approx 1 \times 10^{-2}\, M_\oplus\ {\rm yr}^{-1} \left(\frac{M_p}{10\, M_\oplus}\right)\left(\frac{c_s}{2.0\ {\rm km\ s}^{-1}}\right)^{-1}$$
$$\times \left(\frac{\kappa}{0.1\ {\rm cm}^2\ {\rm g}^{-1}}\right)^{-1}, \quad (4)$$

where we have taken the photosphere pressure as $P_{\rm surf} \approx g/\kappa$, with g being the local gravitational acceleration, κ as the opacity, and the chosen sound speed corresponds to a separation of ∼0.1 AU for molecular hydrogen. Clearly, such a mass-loss rate is not sustainable and it will bring dramatic changes to the planetary atmosphere, an issue we develop later in this paper. For the moment, we only consider the onset of mass-loss. The mass-loss rate drops off exponentially with smaller planet sizes, as the sonic point density depends exponentially on planet sizes (Cranmer 2004). So the importance of our new process depends on the size of the planet when the disk is removed.

In turn, how inflated a newly emerged planet is depends on the race between the cooling/contraction of its envelope and the external process of disk dispersal. If the cooling timescale is much shorter than the disk dispersal timescale, then the planet will contract significantly, rendering post-partum mass-loss insignificant.

The relevant cooling timescale of a gravitational bound object with no internal energy sources (e.g., nuclear burning) is given by the Kelvin–Helmholtz timescale ($t_{\rm KH}$), which for a planet with envelope mass ($M_{\rm env}$) less than the core mass (M_c) is

$$t_{\rm KH} \approx \frac{GM_c M_{\rm env}}{R_p L}, \quad (5)$$

where L is the planet's cooling luminosity. For an embedded planet, one can assume that any cooling flux that reaches the Bondi radius is instantly removed by the external shear flow. This is similar to a planet exposed to a vacuum. So the actual cooling luminosity only depends on the internal structure of the planet, not on its environment.

The near-surface temperature structure determines the cooling luminosity. In the deep atmosphere, heat is mostly advected outward by convective eddies; near the photosphere, this could be accomplished by radiation diffusion. Thanks to stellar heating, the surface temperature of the planet is equilibrated to that of the local blackbody (Equation (2)) if it is exposed, or to the mid-plane disk temperature if it is embedded. This surface searing tends to flatten out the surface temperature gradient to become more isothermal, reducing the heat escape. This situation is similar to that for an irradiated hot Jupiter (Guillot et al. 1996; Burrows et al. 2000; Arras & Bildsten 2006).

The thickness of the radiative zone depends on envelope mass, among other things. The planet atmospheres are fully adiabatic if their internal entropy is as high as the photospheric value—these are the hydrostatic primordial atmospheres as calculated by Pollack et al. (1996) and Rafikov (2006). Because of their large scale height, they contain the least possible amount of mass. To load more mass into these atmospheres, the interiors have to cool to a lower entropy than the surface value.

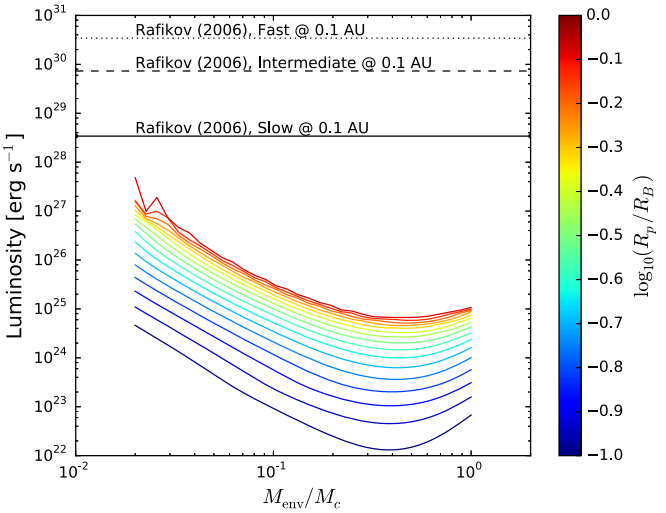

Figure 1. Internal luminosity of a planet with a $5M_\oplus$ rock core and a surface temperature of 900 K (roughly the blackbody temperature at 0.1AU) as a function of the envelope mass fraction. The color of the lines indicates the radius of the planet in units of the Bondi-radius. The three horizontal lines label the expected accretion luminosities from solids in a MMSN disk (Rafikov 2006). At these values, solid accretion easily overwhelm the cooling contraction of the protoplanets.

The lowering of the internal temperature, allied with the surface searing, then entails an ever thickening isothermal blanket.This isothermal layer is effective at blocking the internal heat flow.

As a result, for planets with the same core mass, size, and surface temperature, the cooling luminosity is the largest in ones that have fully convective atmospheres (and the lowest envelope masses), while it decreases rapidly in ones with an isothermal upper layer and accordingly larger envelope masses, as is seen in Figure 1, obtained for planets with a $5M_\oplus$ rock core with a surface temperature of 900 K.[6] The Kelvin–Helmholtz cooling times, for a wide range of models, are presented in Figure 2, where we vary planet photosphere radius (in unit of Bondi radius), envelope mass fraction, surface temperature, and core mass. These values are calculated using the MESA stellar and planetary evolution code (Paxton et al. 2011, 2013), using the setup described in Section 4. All else being equal, one observes that models with a higher envelope mass cool much slower. In addition, higher stellar insolation slows down the cooling contraction. Lastly, cooling is reduced in models that are less extended in size. All of these trends can be explained by the size of the isothermal blanket.

We now turn to discuss the timescale of disk dispersal. There are two timescales of relevance. The first is the timescale a fully grown planet remains embedded, or the remaining disk lifetime after the planet is formed. Since we do not know when planets are formed, we adopt an upper limit to this value, i.e., the full disk lifetime, ∼3–10 Myr (e.g., Haisch et al. 2001; Hernandez et al. 2007; Mamajek et al. 2009). The second is the timescale the disk density drops from its full value to nearly zero. As has become clear by now, the two timescales are not necessarily the same. Disk dispersal—particularly in the inner disk—is known observationally (e.g., Kenyon & Hartmann 1995; Ercolano

[6] The photospheric pressure in these models may differ from that at the disk mid-plane, making these models imperfect for embedded planets. However, luminosity from such a model is still well characterized, as it is largely determined at the radiative-convective boundary (Arras & Bildsten 2006; Wu & Lithwick 2013).

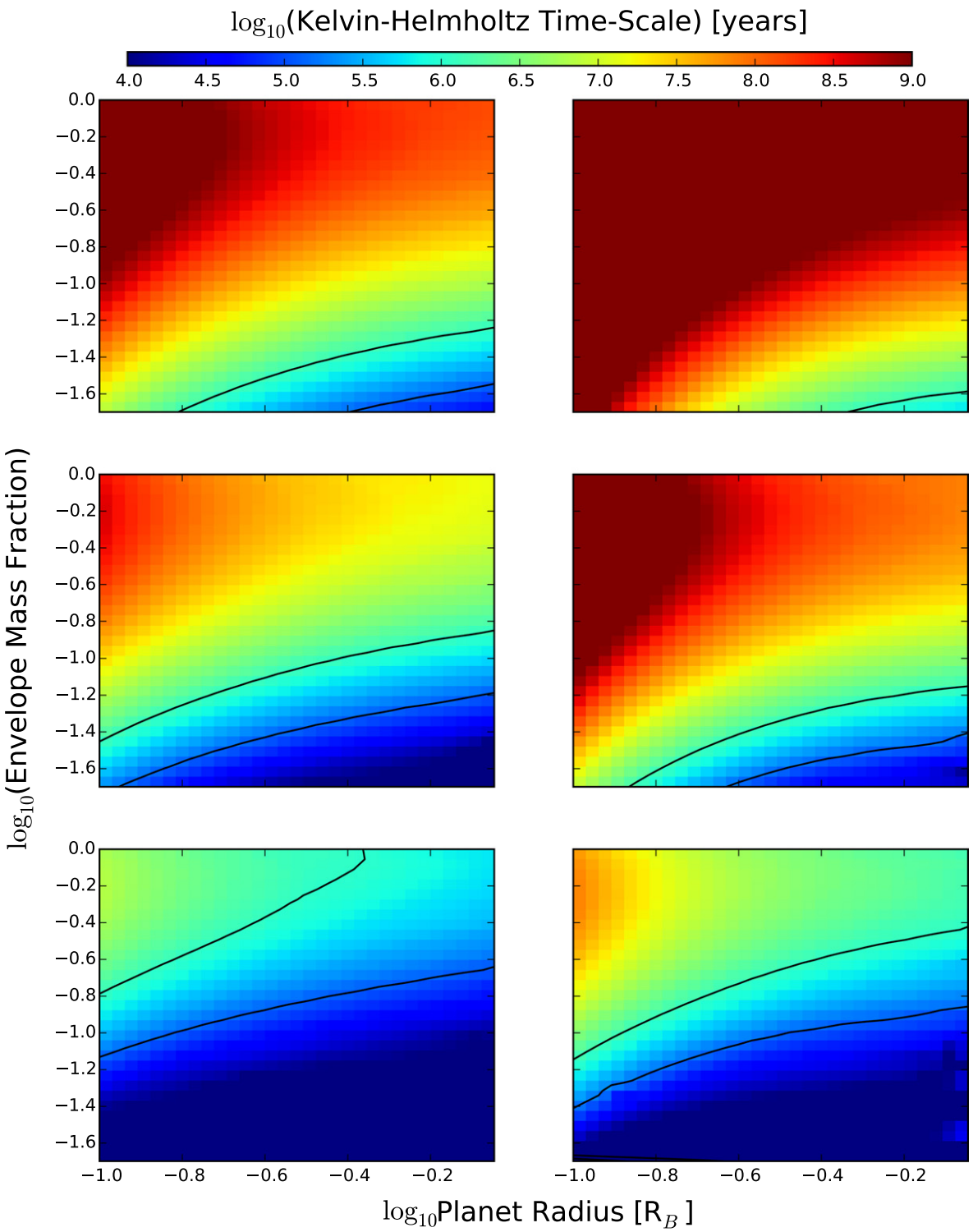

Figure 2. Kelvin–Helmholtz timescale as a function of planet radius in units of the Bondi radius and envelope mass fraction. The solid contours show Kelvin–Helmholtz timescales of 10^6 and 10^5 years. The left panels show planets with an equilibrium temperature of 500 K and the right panels show planets with an equilibrium temperature of 900 K. From top to bottom the panels show planets with core masses of 3, 5, and 10 $M_\oplus$.

et al. 2011; Koepferl et al. 2013) to be at least an order of magnitude quicker than the disk's lifetime, the so called "two timescale" disk evolution. These observations have lead to the development of the photoevaporative-switch dispersal model (Clarke et al. 2001; Alexander et al. 2006; Gorti et al. 2009; Owen et al. 2010, 2011) where photoevaporation of the outer disk carves a gap around 1 AU (for a solar mass star), sabotaging the gas supply to the inner region, causing the latter to rapidly drain onto the central star on its short *local* viscous timescale, which is typically 10^5 years. Alternatively, if the planet is massive enough to open a gap, the local disk clearing timescale can be as short as a few orbital periods (e.g., Crida et al. 2006).

Having established the timescales for cooling contraction and disk dispersal, we can now assess the size of newly emerged planets. Figure 2 shows that a $5M_\oplus$ planet can remain at a size $R_p \sim R_B$ well after disk removal, if its envelope mass fraction is more than ∼10%. This threshold reduces to ∼5% for a $3M_\oplus$ planet, while a $10M_\oplus$ planet can not remain inflated at this size for any relevant envelope mass (this is not unexpected as 10 $M_\oplus$ cores are those typically required for giant planet formation e.g., Rafikov 2006; Piso et al. 2014 in the outer disk). The last observation is consistent with the finding of Lee et al. (2014), where they argue that the envelopes of these planets cool and contract so rapidly that they should undergo runaway gas accretion even while embedded.

Furthermore, one may argue that an embedded planetary core continuously accretes more envelope until the envelope cooling time becomes comparable to the disk lifetime. Adopting a value of 1 Myr, this corresponds to an envelope mass of ∼7% for a $5M_\oplus$ planet at 0.1 AU.

In these discussions, we have overlooked an important detail. We have assumed that the only planet luminosity comes from its cooling contraction. In reality, there is the possibility that the planet can accrete planetesimals (solids) from the surrounding disk. If this is substantial, it could maintain the high entropy of the gas envelope and keep the planet inflated, well past its Kelvin–Helmholtz timescale. As is shown in Figure 1, reasonable estimates for the accretion luminosity (e.g., Rafikov 2006) easily overwhelm the cooling luminosity and may keep the planets inflated longer than estimated in Figure 2.

In summary, we argue that newly emerged low-mass planets ($M < 10M_\oplus$), fully assembled within the inner gaseous disk and with non-negligible envelope masses (∼5%–30%), will remain inflated ($R_p \sim R_B$) when the disk disappears in a rapid timescale of $\sim 10^5$ years, and are thus susceptible to strong winds. This stage of mass-loss occurs after the type of mass-loss studied by (e.g., Ikoma & Hori 2012), and before the EUV/X-ray photoevaporation (e.g., Owen & Wu 2013) that lasts for 100 Myr. We dub this process the "boil-off" and proceed to study it schematically in Section 3 and numerically in Section 4.

3. THE "BOIL-OFF" AND ITS CONSEQUENCES

We now consider the rate of mass-loss and the cooling contraction for a low-mass planet, irradiated by a strong stellar flux after it emerges from the nascent gas disk.

3.1. Mass-loss Rates

A highly inflated young planet, exposed to stellar radiation, is vulnerable to mass-loss. If the wind remains isothermal, as we have assumed, then the appropriate velocity and density profile is given by the Parker wind model (Parker 1958).

Equation (4), generalized for any planet size R_p with $R_p < R_B$, becomes:

$$\dot{M} = 4\pi R_p^2 \rho_{\rm surf} u_{\rm surf} = 4\pi R_p^2 \mathcal{M}_p \left(\frac{P_{\rm surf}}{c_s}\right) = \frac{4\pi G M_p}{\kappa c_s} \mathcal{M}_p, \quad (6)$$

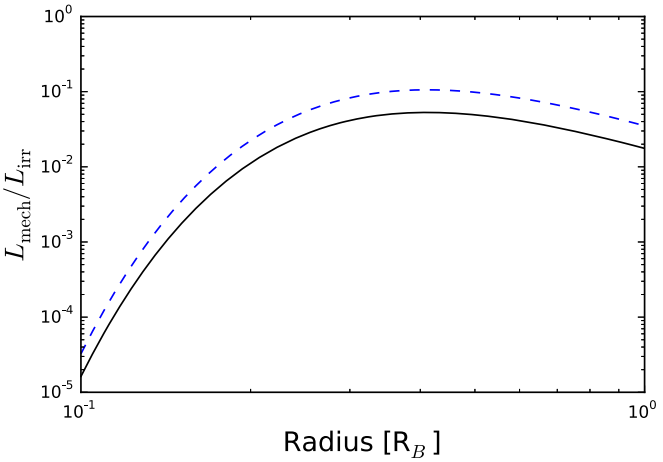

Figure 3. Ratio of mechanical luminosity in a Parker wind, compared to the recived energy from radiation as a function of planet radius. The solid line shows a 10 $M_\oplus$ planet and the dashed line shows a 5 $M_\oplus$ planet, both with an equilibrium temperature of 1000 K. The mechanical luminosity is considerably smaller than the energy from irradiation.

where $\mathcal{M}_p$ is the Mach number of the flow at the planet's photosphere and is only a function of the ratio R_p/R_B, given by:

$$\mathcal{M}_p = \sqrt{-W_0\left[-f\left(R_p/R_B\right)\right]} \quad (7)$$

$$\approx \left(\frac{R_p}{R_B}\right)^{-2} \exp\left(-\frac{2R_B}{R_p}\right) \text{when } R_p \ll R_B, \quad (8)$$

where W_0 is a real branch of the Lambert function (Cranmer 2004) and

$$f(x) = x^{-4} \exp\left(3 - \frac{4}{x}\right). \quad (9)$$

We verify that the energy required to heat up the wind, given the mass-loss rate (Equation (6)), is subordinate to the stellar irradiation for an equilibrium temperature of 1000 K, as is shown in Figure 3 for a 10 and $5M_\oplus$ planet. So energetically, the wind can be heated to isothermal by the star. This energy argument, however, breaks down at an equilibrium temperature of ∼250 K for a $5M_\oplus$ planet and ∼200 K for a $10M_\oplus$ planet. Therefore, at large separations, $\gtrsim$ 1 AU around a Sun-like star, the flow cannot remain isothermal, leading to lower mass-loss rates.

Equation (6) can be used to calculate a mass-loss timescale as:

$$t_{\rm ML} \equiv \frac{M_{\rm env}}{\dot{M}} = \frac{\kappa c_s}{4\pi G} X_{\rm env} \mathcal{M}_p^{-1} \approx 10^3 \text{ years } X_{\rm env} \mathcal{M}_p^{-1} \left(\frac{T_{\rm eq}}{886\text{ K}}\right)^{1/2} \left(\frac{\kappa}{0.1\text{ cm}^2\text{ g}^{-1}}\right), \quad (10)$$

where $X_{\rm env}$ is the envelope mass fraction. In Figure 4 we illustrate how the Mach number at the photosphere, as well as the mass-loss timescale, depend on the ratio of R_p/R_B, by solving the exact Lambert function. But here we provide a schematic argument for the core result. Using the expression for the Mach number when $R_P \ll R_B$ (Equation (8)), we can

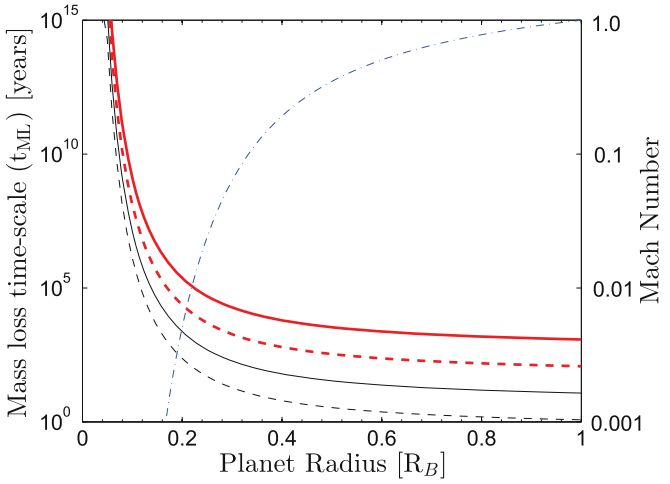

Figure 4. Mass loss timescale (left *Y*-axis) and launch Mach number (right *Y*-axis) as a function of planet radius normalized in terms of the Bondi radius. Thick red lines show the mass-loss timescale for models with $\kappa = 0.01$ cm^2 g^{-1}, whereas thin black lines show the mass-loss timescale for models with $\kappa = 1$ cm^2 g^{-1}; dashed lines indicate models with $a = 0.1$ AU and solid lines indicate models with $a = 1.0$ AU. The thin blue dotted–dashed line shows the launch Mach number. We note the two *Y*-axes are not linked directly.

recast the above equation as

$$\left(\frac{R_p}{R_B}\right)^2 \exp\left(\frac{2R_B}{R_p}\right) \approx X_{\rm env}^{-1}\left(\frac{t_{\rm ML}}{10^3 \text{ years}}\right) \times \left(\frac{T_{\rm eq}}{886 \text{ K}}\right)^{-1/2}\left(\frac{\kappa}{0.1 \text{ cm}^2 \text{ g}^{-1}}\right)^{-1}. \quad (11)$$

So at small R_p/R_B, the mass-loss is exponentially sensitive to the value of R_p/R_B. Alternatively, one can say that the final radius where mass-loss effectively stalls is only logarithmically sensitive to the exact model parameters, and is always of the order of $R_p/R_B \sim 0.1$. As can be observed in Figure 4, this is indeed the point where the mass-loss timescale sky-rockets to exceptionally long timescales.

So once the confining pressure of the disk is lifted the planet's atmosphere—although in roughly dynamical equilibrium—will undergo rapid mass-loss. Such a mass-loss, if happening at a pace faster than the intrinsic cooling contraction of the planet, as is indeed the case in Figure 4, will dominate the thermal evolution of the planetary atmosphere.

3.2. Consequences for Thermal Evolution

Just like evaporation from the skin cools us in the summer heat, the rapid mass-loss from young planets will lead to dramatic cooling and contraction.

In a planet without mass-loss, its internal heat is transported outward by a combination of convection and radiative diffusion. The heat leakage, and hence the rate of cooling contraction, is limited by the bottle-neck in this transport process, i.e., the outer radiative zone. This is the reason behind the results shown in Figure 2. Mass-loss alters this picture. The outflow advects thermal energy at a rate

$$L_{\rm adv} \approx \frac{\gamma}{\gamma - 1}\dot{M}c_s^2 \sim 10^{26} \text{ erg s}^{-1}\left(\frac{\dot{M}}{1 \times 10^{-5} M_\oplus \text{ yr}^{-1}}\right) \times \left(\frac{c_s}{3 \times 10^5 \text{ cm s}^{-1}}\right)^2, \quad (12)$$

where γ is the ratio of specific heats. This flux easily overwhelms the cooling luminosities of low-mass planets (Figure 1). As a result, the hot interior of the planet can shed its energy at a rate much higher than that permitted by the radiative bottle-neck. The planet cools down in a hurry.

This cooling reduces the thermal support for the atmosphere and it contracts. The contraction reaches $R_p \sim 0.1R_B$ within a few $t_{\rm ML}$. This effectively shuts off the mass-loss and cooling resumes the original pace in which the radiative bottle-neck is important (Lopez & Fortney 2013; Owen & Wu 2013). Unlike the case of no mass-loss, where $t_{\rm KH}$ is always of order the age of the planet, we now have a planet which is young in age, but "looks" old. Specifically, it has a Kelvin–Helmholtz timescale that is considerably larger than its age.

3.3. Final Envelope Mass

Knowing the initial and final radius of the planet envelope, we can estimate the amount of mass-loss using an energy argument.

For the initial state, the binding energy of the envelope is

$$U_i = -A_i\frac{GM_cM_{\rm env}^i}{\alpha R_B}, \quad (13)$$

where A_i is an order unity constant and is determined by the central concentration in the envelope. α is a parameter ($\leqslant 1$) that represents the initial radius of the planetary atmosphere in terms of the Bondi radius. After the episode of mass-loss, the envelope has shrunk to a radius of $0.1R_B$ and the binding energy of the envelope is now

$$U_e = -10A_e\frac{GM_cM_{\rm env}^f}{R_B}. \quad (14)$$

where A_e is also an order unity number that describes the central concentration of the new state. As the mass-loss rate is exponentially sensitive to planet radius, we expect that most of the loss occurs when the planet was at its initial size, and this requires a binding energy release of

$$U_{\rm lost} \approx \frac{GM_c(M_{\rm env}^i - M_{\rm env}^f)}{\alpha R_B}. \quad (15)$$

Assuming that the potential energy difference between the initial and the final state is all used to drive the Parker wind, or, $U_i - U_e = U_{\rm lost}$, we can solve for the final envelope mass as

$$M_{\rm env}^f = \left(\frac{A_i + 1}{10\alpha A_e + 1}\right)M_{\rm env}^i \approx 0.2\alpha^{-1}M_{\rm env}^i, \quad (16)$$

where we have taken $A_i \sim A_e \sim 1$.

In this discussion, we ignore two other energy terms. One is the energy gain from the stellar insolation, which can be orders of magnitude larger than the planet's internal luminosity; and one is the energy loss from convective/radiative transport. The

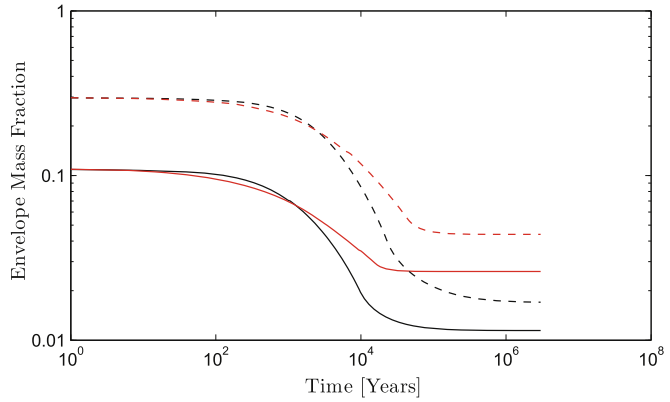

Figure 5. Mass evolution for models with a 5 $M_\oplus$ core. The red lines are for models with an equilibrium temperature of 500 K while the black lines are for 900 K. The solid and dashed lines stand for models with initial envelope fractions of 10% and 30%, respectively. All models start with a radius $R_p = R_B$.

latter, as we have argued, is subordinate to the advective energy flux due to mass loss and can be safely ignored (also see numerical evidences in Section 4). The first assumption, however, takes some considerations.

First, stellar heating is essential to drive the Parker wind. It continuously heats the gas above the photosphere, allowing them to reach escape velocity. Without it, the atmosphere will happily remain at a hydrostatic equilibrium. However, stellar heating is only a minor energy source for mass-loss, not the driving engine. Stellar heating provides the final push to take a gas parcel from the photosphere to infinity, and the pressure loss caused by the outflow allows gas to rise up from below. The increase in its binding energy is provided by the gravitational contraction of the underlying gas. If we include the energy gain due to stellar irradiation into our simple analysis, $U_{\rm irr} = \epsilon\,(R_B/a)^2 L_* t_{\rm boil}$, where L_* is the stellar luminosity, $t_{\rm boil}$ is the length of the boil-off phase and ϵ a small pre-factor $\ll 1$, we find,

$$M_{\rm env}^f \approx 0.2\alpha^{-1} M_{\rm env}^i - \epsilon\left(\frac{R_B}{a}\right)^2 \frac{L_* t_{\rm boil} R_B}{G M_c}. \quad (17)$$

This shows that stellar irradiation can increase the mass-loss slightly, with the strongest effects for small separations and low core masses.

In numerical simulations, we frequently find that the final envelope mass is some 10% or less of the initial mass (Figure 5), indicating that stellar irradiation is a sub-dominant energy source.

4. NUMERICAL CALCULATIONS

We simulate the thermal and dynamical evolution of a spherically symmetric planetary envelope, subject to the boundary conditions of stellar irradiation and mass-loss. The gas is optically thick to radiation ($\tau \geqslant 2/3$) so that the radiation field and the fluid are in local thermal equilibrium. Additionally, we assume that the radiation transport takes place in the static diffusion limit, i.e., $v/c \ll \lambda_p/\ell$ (where λ_p is the mean free path of the photons and ℓ is the scale length of the atmosphere), a condition easily satisfied in our problem.

4.1. Numerical Method

We use the MESA code (Paxton et al. 2011, 2013) to solve this radiation-hydrodynamics problem. This code traces the evolution of any mass shell inside the planet, as is dictated by the equations of mass conservation, momentum conservation, and energy conservation, subject to suitable boundary conditions. This is valid so long as the simulated domain contains no shocks and sonic points. In other words, we cannot follow the Parker wind through its escape process. Instead, we have to independently specify a mass-loss rate at the outer boundary of the planet. Since MESA is essentially a Lagrangian hydrodynamics code (namely, following the mass element), this is not straightforward to implement and we discuss this below.

4.1.1. Implementation of Mass-loss

To specify the mass-loss rate in MESA, one removes a certain amount of mass from the top layers (we take the surface to be the photosphere with $\tau = 2/3$ to the outgoing radiation) at the beginning of each time-step and then lets the system readjust, as is described in detail in the MESA code paper (Paxton et al. 2011).

In our implementation, we assume that the flow above the photosphere follows the isothermal Parker wind solution with a temperature equal to the equilibrium temperature $T_{\rm eq}$ (Equation (2)) and a mass-loss rate as in Equations (6)–(7).

At early times when the planet is highly inflated ($R_p \sim R_B$), we find this rate may formally exceed the so-called "energy-limited" rate, the rate at which all stellar flux is converted into kinetic energy in the wind. For these short periods, we cap the mass-loss rate at 10% of the energy-limited rate. This choice makes little difference to the evolutionary tracks.

One also has the freedom in how to implement the mass-loss term in detail, either implementing over a few grids near the photosphere, or spreading it across the surface scale heights. We have experimented with this and found that provided the loss term is smooth, small, and does not remove significant mass from where the contraction of the atmosphere is taking place, it does not matter.

4.1.2. Implementation of Flux Boundary Condition

The outer boundary is set at the $\tau = 2/3$ surface to the outgoing radiation. To include stellar irradiation, we adopt the MESA $F_* - \Sigma$ implementation (Paxton et al. 2013). This consists of depositing a total irradiation flux of $F_*/4$ uniformly down to a column density Σ, where we choose $\Sigma = 250\,{\rm g\,cm^{-2}}$, as is appropriate for an opacity of $\kappa_v = 4 \times 10^{-3}\,{\rm cm^2\,g^{-1}}$ to the incoming stellar flux, the value suggested by Guillot (2010) for Sun-like stars.

The $F_* - \Sigma$ method of including irradiation in planetary evolution has been shown to provide good agreement to other boundary conditions in Paxton et al. (2013), when mass-loss is not dynamically important. It differs from the usual approach of applying a gray or semi-gray approximate solution to the atmosphere (e.g., Guillot 2010), as used by Owen & Wu (2013). It is necessary in this problem because the energy balance in the upper layers of the atmosphere must be taken into account explicitly, including PdV cooling and advection. However, for the sake of simplicity, we identify numerical models by their respective $T_{\rm eq}$, not their F_* values.

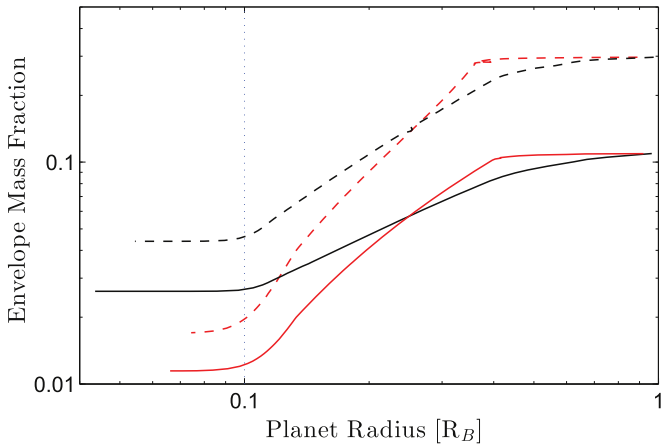

Figure 6. Evolution of the same models in Figure 5, shown in the radius–mass plane, where the planet's radius is scaled to the Bondi radius. A radius of 0.1 R_B is shown as the thin dotted line.

4.1.3. Initialization

We initialize our models as hydrostatic planets, with a radius of R_B ($\alpha = 1$), with a chosen envelope mass and core mass. The planet models were created by building a slightly larger than required planet (at a higher entropy) that was then allowed to cool to the required value. The core radius is determined assuming a pure rock composition that follows the mass–radius relation from Fortney et al. (2007). We include radioactive heating from the core as described in Owen & Wu (2013) but it has negligible impact; moreover, we neglect heating from the core's heat capacity because over the short timescales of interest the core is unable to transfer heat to the envelope (see Lee et al. 2014, for a detailed discussion). Specifying these parameters uniquely determines the properties of the planet's atmosphere. We then switch on the hydrodynamic terms and mass-loss and let the models adjust to a new equilibrium (typically this results in a small reduction in radius). We then evolve the model forward using a time-step that satisfies the convergence criterion described in Paxton et al. (2011) as well as limiting the relative change in envelope mass to $<10^{-3}$ each time-step. We stop the evolution after 3 Myr, at which time mass-loss has practically ceased in all our calculations. Given the number of simplifications made in order to perform the calculations, we perform a series of tests in the Appendix to ensure that our results are robust.

We consider models with two different initial envelope mass-fractions, 10% and 30%, compatible with those found by core-accretion models at small separations (e.g., Bodenheimer & Lissauer 2014; Lee et al. 2014) and have long enough cooling times to remain bloated even at disk dispersal. We note the true mass fraction, at the time of disk dispersal, is likely determined by the fluid mechanics and the thermodynamics around an embedded planet and is beyond the scope of this work. We study three core masses of 3, 5, and 10 $M_\oplus$ and two equilibrium temperatures of 500 and 900 K.

4.2. The Results

As is shown in Figure 5, the evolution of all models is similar: the planet's atmospheres contract, lose mass, and cool on a timescale of the order of 10^5 years. The internal contraction provides energy to lift up the outer envelopes. The mass-loss drops off exponentially with planet size as discussed in Section 3.1, and after a few 10^5 years, when the planet's radius reaches $\sim 0.1 R_B$ (Figure 6), mass-loss ceases entirely and the planet cools down normally. At this point, the final envelope mass is ~10% of the initial one, consistent with the estimate in Equation (16).

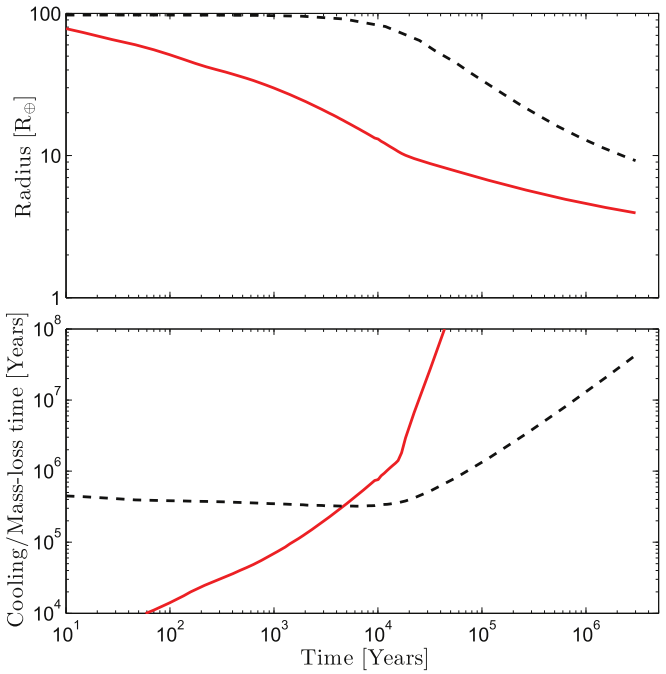

Figure 7. Radius and timescale evolution for a 5 $M_\oplus$ core and an initial envelope mass fraction of 10% , at an equilibrium temperature of 500 K (the solid red line in Figure 5). The top panel shows its radius evolution, with the dashed curve representing a similar model where there is no mass-loss. The bottom two panels shows how the Kelvin–Helmholtz timescale (dotted–dashed) and the mass-loss timescale (solid) evolve as a function of time and envelope mass fraction. By the time the mass-loss ceases (~1 Myr), the planet looks like one that has cooled for ~50 Myr.

We focus on one model to gain more insight. Figure 7 presents the evolution of a planet with a $5M_\oplus$ core, an initial mass fraction of 10% and at an equilibrium temperature of 500 K (the red solid line in Figure 5). Compared to a similar model without an imposed mass-loss, the contraction of our model is much more rapid, indicating that the energy for the mass-loss indeed obtains from internal gravitational contraction. The mass-loss timescale (inverse of the mass-loss rate) starts low but sky-rockets to an astronomically long timescale as the planet's radius shrinks. The Kelvin–Helmholtz time, defined as the timescale to radiate the envelope's binding energy at the current luminosity,[7] lies always above the system age, again indicating that the binding energy is not primarily lost by radiative/convective transport, but by advection. By the time mass-loss has stopped (~1 Myr), the planet has a Kelvin–Helmholtz time of ~50 Myr. It has "aged" prematurely.

We present snapshots of the fluid velocity and luminosity profiles for the same model in Figure 8. Initially the planet's envelope is expanding so fast, it completely absorbs the planet's internal luminosity and converts it into *PdV* work, resulting in negative luminosity in the surface layers. This layer reaches much deeper than the penetration depth of the stellar irradiation, again proving that the main source of energy for the

[7] We pick this to be the maximum luminosity in the envelope, rather than the surface luminosity as the latter can sometimes be negative (Figure 8).

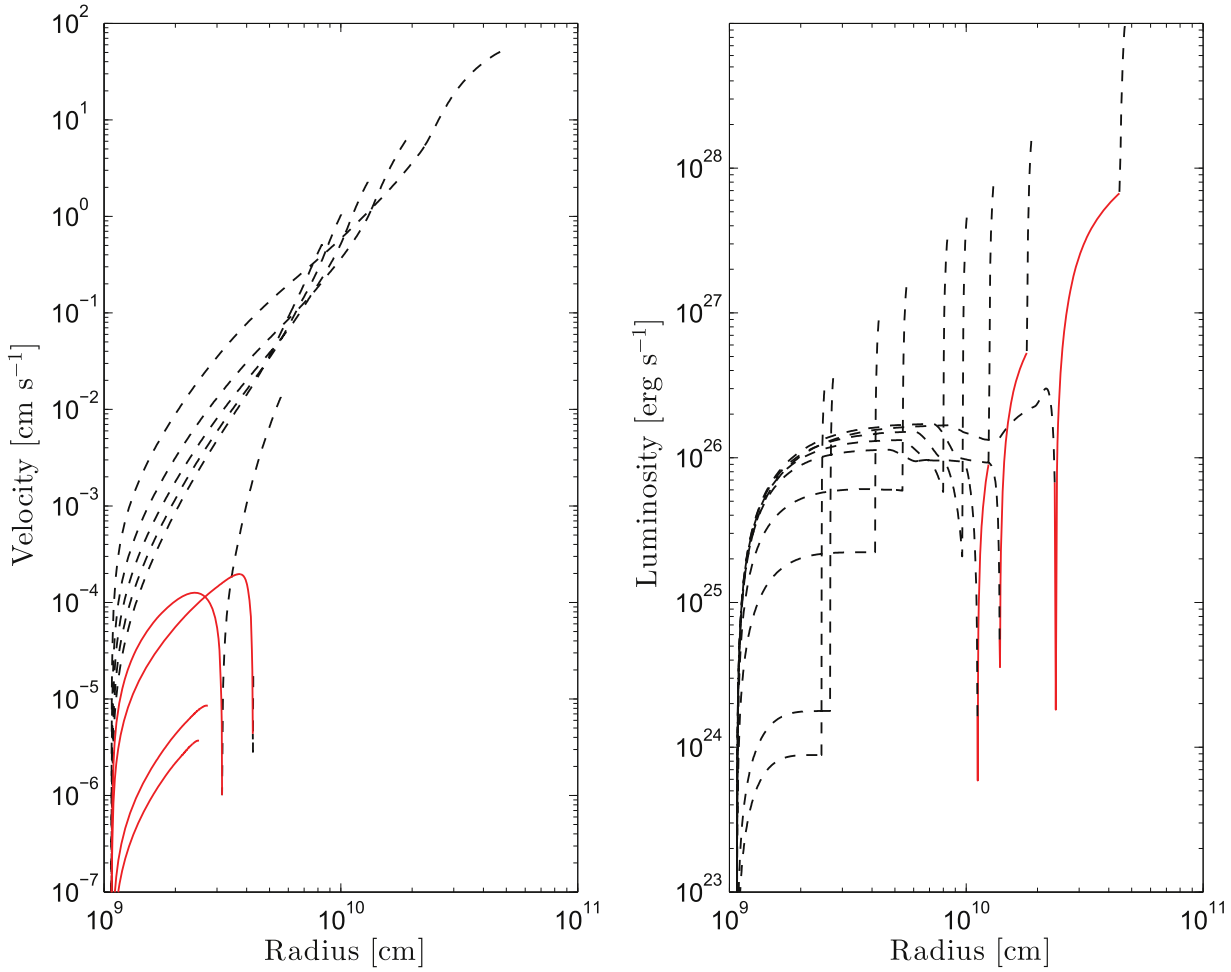

Figure 8. Snapshots of the velocity and luminosity profiles as a function of radius for a model with a $5M_{\oplus}$ core, an initial mass fraction of 10%, and at an equilibrium temperature of 500 K (the model shown in Figure 7). From top to bottom, the following times are shown: 10^2, 10^3, 10^4, 3×10^4, 6×10^4, 10^5, 3×10^5, 10^6, and 3×10^6 years. Solid lines represent negative values, while dashed lines represent postive values. A negative luminosity represents an inwardly directed radiative flux. The large luminosity spike at the surface arises as we are explicitly adding the heating from stellar irradiation and is representative of the re-radiated stellar flux. The change in sign close to the planet's surface is abrubt and unresolved, as a result of our simplified $F_* - \Sigma$ method for including stellar irradiation. However, as discussed in the Appendix this simplified treatment does not impact our calculations.

mass-loss is the planet atmosphere's internal luminosity. By losing mass, the planet is then able to cool and contract significantly such that it shuts off the mass loss. Within 1 Myr, the planet's luminosity has dropped by a factor of 100, and its envelope now radially contracts (as opposed to outflow).

Finally, in Figures 9 and 10 we present composite results for the envelope mass and the cooling time after 3×10^6 years of evolution. We see that models receiving a stronger stellar insolation lose more mass—roughly by a factor of 2 between the 900 K and the 500 K models. We also see that less massive planets have a harder time retaining their envelopes. This difference is expected from the expression given in Equation (17), where stronger irradiation and lower core masses lead to slightly more mass-loss, although we note that since this effect is small and the planets cool significantly, energy input from stellar irradiation is a sub-dominant effect. In some cases, envelopes around the lowest mass planets ($3\ M_{\oplus}$) can be blasted away so completely that they appear as "naked" cores. Furthermore, by the end of 3 Myr, all planets have a cooling time in the range of 4×10^7–10^8 years, approximately ~20 times longer than one would have predicted if the planets cooled purely by gravitational contraction.

5. DISCUSSION

We discuss how our new process relates to previous works on mass-loss of planetary envelopes, and what our work implies for the observed planetary properties. We connect this process with the first stage of mass-loss, which occurs while the disk is dispersing (Ikoma & Hori 2012), and with the later stage driven by EUV/X-ray photoevaporation.

5.1. Relation to Ikoma & Hori (2012)

Ikoma & Hori (2012) considered the evolution of an embedded low-mass planet as the background disk density and pressure slowly declined. They found that the planetary atmosphere was eroded, more extremely so if an additional heat source keeps the planet puffy. For the latter, they invoked the cooling luminosity from the solid core. However, Lee et al. (2014) argued they may have adopted a cooling luminosity that is too large—with an assumed cooling time of ~10^5 years for a core the size of the Earth—this may have grossly overestimated the transport ability of either heat conduction or mantle convection.

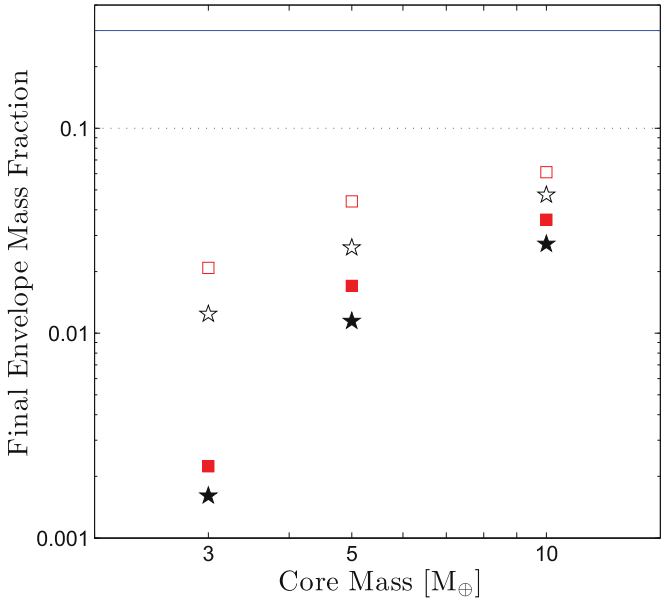

Figure 9. Final envelope mass as a function of core mass. Red symbols have an equilibrium temperature of 500 K, whereas black symbols are 900 K. Open symbols initially had a 30% envelope fraction (shown as the thin solid blue line) and the filled symbols initially had a 10% envelope fraction (shown as the thin dotted blue line). Assumed to start at a radius of R_B, all models lose substantial amounts of envelopes, with the effect being more drastic for planets with a lower core mass, a stronger irradiation, and a less massive envelope.

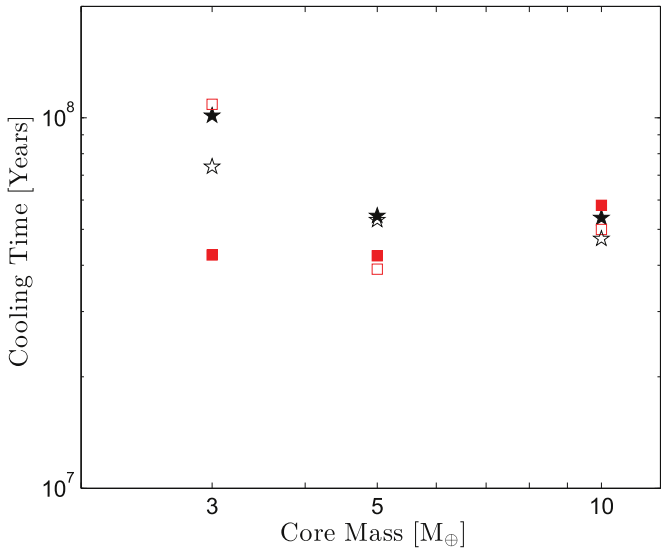

Figure 10. Same as Figure 9, but for the cooling time at the end of 3 Myr. The "boil-off" removes internal energy from these planets, allowing them to cool off much faster than their ages indicate.

Ikoma & Hori (2012) are concerned with the mass-loss during the disk dispersal (with a timescale $\sim 10^5$ years), while we are interested in what happens afterward. So the process they investigated is a natural predecessor to the one studied here, and it provides the initial input for our model.

Physically, their mechanism is similar to ours, except in details, at least in the case of no additional heat source. By reducing external pressure confinement gradually, Ikoma & Hori (2012) observed a mass-loss that likely occurs through a sub-sonic breeze.[8] In this work, we are concerned with a transonic wind. Both flows are similar in that they both draw energy from the gravitational contraction (when core cooling is not important). Above the photosphere, our wind is propelled by stellar heating, while their mass-loss is powered by the pressure differential between the atmosphere and the background.

How important is this early episode of mass-loss? Or, in other words, when does the breeze stop and the wind start? We speculate that the transition may occur well before the disk becomes so optically thin that the outflow can be heated by the star. The infrared glow from the background disk may be already sufficient to keep the outflow roughly isothermal. Moreover, the decay of the disk's confining pressure becomes irrelevant once the ram pressure in the outflow is strong enough. This occurs before the gas mean free-path becomes as large as the planetary radius, a threshold set by Ikoma & Hori (2012) for the termination of their simulations. However, in order to model this properly, one needs to improve upon the modeling in Ikoma & Hori (2012) by including the hydrodynamics terms explicitly in the evolution equations, and to include the breeze solution explicitly. Ultimately a single simulation that follows the protoplanet all the way through disk dispersal and boil-off is required to assess the relative importance of the processes in shaping the planet population.

We note that in some of our numerical calculations the mass-loss timescale is similar to the disk clearing time scales and as such our results will be sensitive to when this crossover takes place. Specifically, if disk pressure drops quicker than the "breeze" solutions can transfer mass sufficiently to maintain equilibrium, then the planet will launch a Parker wind early; however, if the disk pressure drops slowly enough, the "breeze" can remove sufficient material to make the wind phase (boil-off) less important. We note that the breeze mass-loss rates are always lower than those driven by the Parker wind, thus we suspect the "boil-off" phase will dominate the total mass-loss.

5.2. Relation to EUV/X-Ray Driven Evaporation

More mass-loss can occur at the end of our simulations, after the planet has contracted to a radius of $R_p \leqslant 0.1 R_B$. The ionizing radiation (EUV/X-ray, as opposed to continuum radiation considered here) from the star can elevate the temperature in the upper layers to $\sim$5000–10^4 K, as opposed to the blackbody temperature considered here (Owen & Jackson 2012). The corresponding sound speed can approach the escape velocity at the photosphere, even for a more compact planet. This then drives a photoevaporative outflow. This has been shown to be particularly significant for *Kepler* planets inward of $\sim$0.2 AU from the host stars and can explain the smaller sizes of these close-in planets (Lopez & Fortney 2013; Owen & Wu 2013). The atmosphere of these planets can be completely removed, consistent with the high bulk densities observed in objects like CoRoT-7b (Hatzes et al. 2011), Kepler-10b (Batalha et al. 2011), Kepler-36b (Carter et al. 2012) and others (Weiss & Marcy 2014).

Owen & Wu (2013) demonstrated that this mode of mass-loss is most significant in the first $\sim$100 Myr, mostly because this is when the host star is more chromospherically active (and hence stronger ionizing radiation), but also because this is when the planet is more extended (with a smaller surface

[8] However, this process is not explicitly modeled in their work and as a result, their mass-loss rate may not be physically self-consistent.

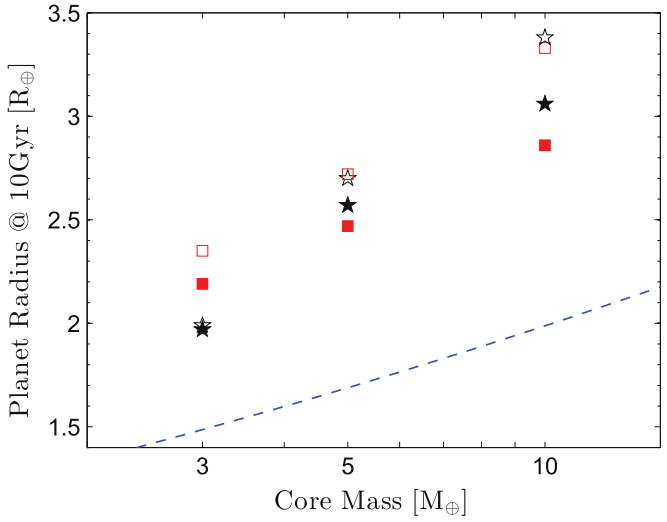

Figure 11. Same as Figure 9, but for the final planet radius after 10 Gyr of cooling contraction. For planets less massive than $10M_{\oplus}$, the final radii tend to cluster around $2.5R_{\oplus}$, the radius observed for a large number of *Kepler* planets. Here, the dashed line indicates the radius of the planetary core.

escape velocity). Short of knowing the initial radii for the planets, they explored models with a range of initial cooling times (from 3 to 100 Myr), where a shorter cooling time corresponds to models with a more extended photosphere. They concluded that the models with the shortest cooling time lose the most mass, with the difference being more significant for lower mass envelopes (Figure 4 of Owen & Wu 2013).

This provides the context for our results in Figures 9–10. They quantify the initial conditions for the later photoevaporative flow, just like results from a study like Ikoma & Hori (2012) can do for our work here. The early episode of mass-loss, propelled by continuum stellar radiation and powered by gravitational contraction of the planet, cools the planet to a smaller radii, affecting the outcome of later photoevaporation. As such, we argue that a coherent study where one follows the evolution of the planet envelope through these different stages, instead of studying them independently, would be needed to predict the final envelope mass one observes.

5.3. Applications to Kepler Planets

Despite being only one of the three possible steps in mass removal, the "boil-off" process discussed here may explain some of the observed features in *Kepler* planets.

It may help explain the dramatic deficit of planets with sizes above $\sim 2.5R_{\oplus}$ in the *Kepler* catalog. This radius corresponds to an envelope mass of $\sim 1\%$ for planets that have cooled for a few Gyr. Limited by the transit technique and the mission duration, this catalog mostly contains planets inward of ~ 0.5 AU ($T_{\rm eq} \approx 400$ K). For these planets, Figure 9 shows that, even if they were started with much more massive envelopes (10%–30%), the "boil-off" would have left them with much punier envelopes (of order 1%) after a few Myr. Moreover, the final envelope mass, at the same location, is found to scale roughly with the core mass. As a more massive core exerts a stronger gravity on the envelope and compresses it more, this correlation leads to a further convergence in final planet radii, as is shown in Figure 11.

In contrast, planets outside this distance range will experience less mass-loss (see Figure 5) and they may retain most of their primordial envelopes. In other words, we predict that there are relatively more neptunes, with envelope mass fractions of tens of percent, outside the $\gtrsim 1$ AU range. This could be tested by future transit missions.

We can contrast these predictions of the boil-off against those from EUV/X-ray photoevaporation (Owen & Wu 2013). The latter effect is mostly limited to separation $\lesssim 0.2$ AU. If the latter acts alone, one would expect an abundance of Neptunes outside 0.2 AU, closer than our above prediction for the "boil-off." This difference may already be discernible in the *Kepler* data. However, detailed comparison between theory and observation needs to take into account the planet mass, which is largely unknown at the moment, especially for planets outward of 0.2 AU.

Are there Neptunes within 1 AU? We find that *Kepler* data show a smattering of Neptune-like planets within this distance. How could these planets have escaped the "boil-off"? We speculate that their cores are more massive than $\gtrsim 10\ M_{\oplus}$ (see Figure 9) and therefore can hold on to their envelopes better. This conjecture is supported by the general mass–radius relationship of $M \propto R$, as is obtained from TTV and RV mass measurements (Wu & Lithwick 2013; Hadden & Lithwick 2014; Weiss & Marcy 2014; Wolfgang et al. 2015). The fact that larger planets do tend to have more massive cores is consistent with the "boil-off" process. Conversely speaking, the "boil-off" *helps* explain the observed mass–radius relation.

However, such an explanation is incompatible with the presence of a few Neptune-like planets that have unusually low densities (Kepler-51, Masuda 2014) (Kepler-79, Jontof-Hutter et al. 2014); (Kepler-87, Ofir et al. 2014). These masses are typically of the order of $2–5M_{\oplus}$, within the range where we predict the "boil-off" should have carried off most of their envelopes. They may be counterevidence for our theory, but we hope their mass determinations (all TTV inferences) can be confirmed by radial velocity studies. Furthermore, since they do not appear to be a dominant population (through the radius distribution), they may have a different origin (Lee & Chiang 2014).

Finally, Rogers (2014) suggest that all planets with radii $\lesssim 1.6\ R_{\oplus}$ are predominantly rocky. A $1.6\ R_{\oplus}$ rock planet is roughly a $4\ M_{\oplus}$ (Fortney et al. 2007). We note that this process may play a role in shaping this result. However, we need to be cautious as one needs to perform a more detailed study that factors into the separation distribution, as normal evaporation (e.g., Owen & Wu 2013) is able create this as well. Thus, in order to untangle the true origin of the solid to H/He transition —which may turn out to be a separation dependant statement— further modeling is required.

6. CONCLUSION

We now know that there are three stages of envelope mass-loss: while the planet is embedded in the disk; soon after the disk disperses; and while the planet is contracting, with typical durations of $\sim 10^5$ Myr, 10^5 Myr and 10^8 Myr, respectively. These processes combine to sculpt the final radius and mass distributions of the close-in low-mass planets.

We have presented and investigated the second stage, dubbed the "boil-off" phase, whereby an irradiated, inflated ($R_p \sim R_B$) low-mass planet loses its envelope and contracts quickly. Our investigation can be summarized as follows.

1. We argue that many low-mass planets should have photospheric radii $R_p \sim R_B$ by the time disk disperses, due to their naturally long Kelvin–Helmholtz timescales, and perhaps aided by the small amount of heat input by planetesimal accretion. As such, they are subject to the "boil-off." The primary energy source for the mass-loss is the binding energy of the planet itself, with the continuum stellar irradiation acting as a "catalyst" for the mass-loss.
2. Due to the characteristics of an isothermal wind, this "boil-off" will cease when the planet has contracted to within $0.1R_B$.
3. Order of magnitude energetic considerations show that by this time, the envelope mass has reduced to $\sim 0.2/\alpha$ of its initial mass, where α is the initial radius in units of R_B.
4. We find that this process leads to extreme cooling of the planet. Within a Myr, the planet would have cooled down to a state that is only reached after ~100 Myr of evolution without mass-loss.
5. Relatively speaking, mass-loss is more severe for planets with lower core masses, and for planets subject to stronger stellar irradiation. Planets more massive than $10M_\oplus$ should be less affected by this process, so do planets that have accreted so much gas they have undergone runaway gas accretion.
6. This process could remove the massive envelopes of Neptune-like planets that are inward of ~0.5 AU, explaining the observed steep fall-off in planet numbers above a size of $2.5R_\oplus$, provided planet formation results in initial envelope mass fractions of order tens of percent, as is suggested by recent simulations and basic timescale arguments, (e.g., Lee et al. 2014; Lee & Chiang 2014). A corollary is that we expect neptunes to be more common at larger separations.
7. This process may also be responsible for the observed mass–radius relation ($M \propto R$). More massive planets can retain more of their envelopes, leading to larger sizes. However, EUV/X-ray photoevaporation can also lead to the same trend. Work is needed to identify the relative importances of these processes.

To predict the final envelope mass for planets, one need to model the formation, the disk dispersal, the "boil-off", and the subsequent photoevaporation process, a task that may now be within reach.

We thank the anonymous referee for a thorough and insightful report. J.E.O. acknowledges support by NASA through Hubble Fellowship grant HST-HF2-51346.001-A awarded by the Space Telescope Science Institute, which is operated by the Association of Universities for Research in Astronomy, Inc., for NASA, under contract NAS 5-26555. Y.W. acknowledges financial support from NSERC. We are grateful to Eugene Chiang for fruitful discussions.

APPENDIX
TESTS OF NUMERICAL APPROACH

In order to model the "boil-off" phase with the MESA stellar/planetary evolution code we have made a number of simplifying assumptions in order to model the radiative transfer and mass-loss. Therefore, it is important to check that these approximations are not driving our results and our results are robust to the exact tuning parameters chosen in MESA. When including mass-loss from the boil-off process in the calculations we assume that the flow is isothermal and can be approximated by a Parker wind which we do not attempt to explicitly model. Instead the outer boundary for our models is the photosphere to the outgoing IR radiation and we apply the mass-loss as a sink term at the top of the envelope. We can check that the outer layers of our model (below the photosphere) are quasi-isothermal and close to the equilibrium temperature, indicating that our choice of a Parker-wind is an appropriate first step. If, for example PdV work of the expanding upper atmosphere (below the photosphere) could not be compensated for by the radiative heating, then the atmosphere would significantly cool below the equilibrium temperature, being closer to adiabatic, a Parker wind would not be an appropriate model.

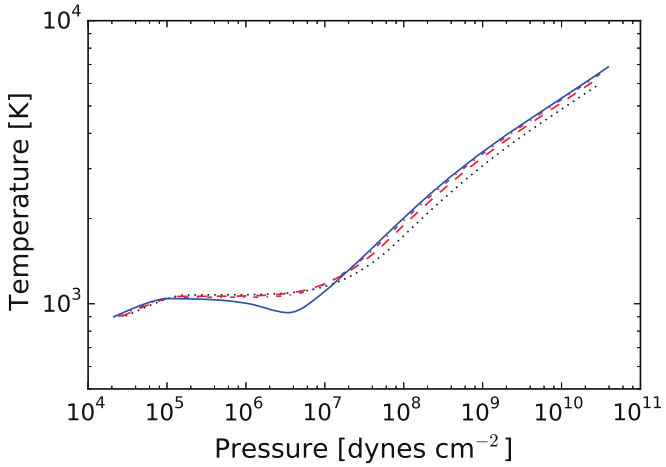

Figure 12. Pressure temperature profiles for the calculation of a planet with an initial envelope mass fraction of 30%, core mass of 5 $M_\oplus$ at an equilibrium temperature of 900 K. They are shown at times of 3.7×10^4 (solid), 8.3×10^4 (dotted–dashed), 1.8×10^5 (dashed) and 4.4×10^5 (solid) years.

Snapshots of the pressure–temperature profile are shown for an evolving planet in Figure 12, which show the outer layers of the envelope are quasi-isothermal during the evolution close to the equilibrium temperature of 900 K.

As discussed in Section 4, the mass-loss is included as a sub-step in the evolution of the planet's envelope where mass is removed from the upper layers. As noted above, occasionally at early times the mass-loss rate given by the Parker wind occasionally exceeded the "energy-limited" rate and we included an efficiency factor of 10% to correct this. In Figure 13 we show the evolution of the envelope mass fraction for the model with a 5 $M_\oplus$ core and initial envelope mass fraction of 30% where this efficiency is varied with values of 10% (solid) and 100% (dotted–dashed), while this obviously effects the evolution at early times, the evolution is identical at late times with the final envelope mass fraction are within <0.3% across all the simulations.

We can also check that the amount of the atmosphere we are smoothing the mass-loss over does not effect our results. In MESA the range of the envelope that material is removed every sub-step is controlled by the `min_q_for_k` parameters that set the mass fraction of the upper envelope over which material is removed. The standard value is that any mass is removed from the top (by mass fraction) <0.5% of the atmosphere, which is used in all our previous calculations. In Figure 14 we show the

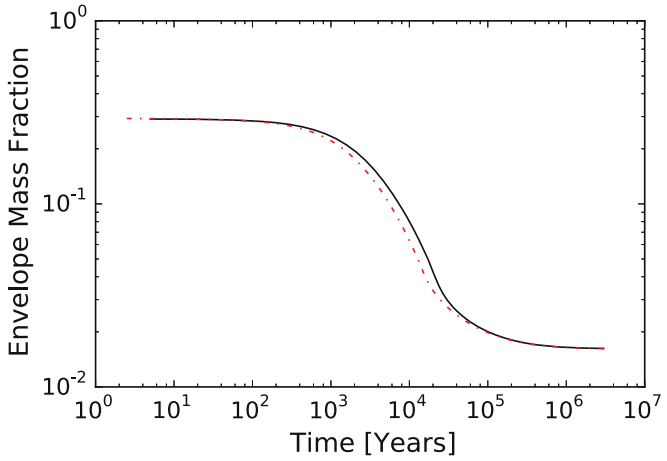

Figure 13. Evolution of the envelope mass fraction for the model with a 5 $M_\oplus$ core and initial envelope mass fraction of 30% at an equilibrium temperature of 900 K. The different lines show cases where the mass-loss rates is capped to different values of the "energy-limited" rate at early times: 10% (solid—the standard value used in our work) and 100% (dotted–dashed). The evolution at early times is different, but at late times the evolution is identical and the final envelope mass fractions found are consistent to within <0.3%. Therefore, we are confident the efficiency choice is not driving our results.

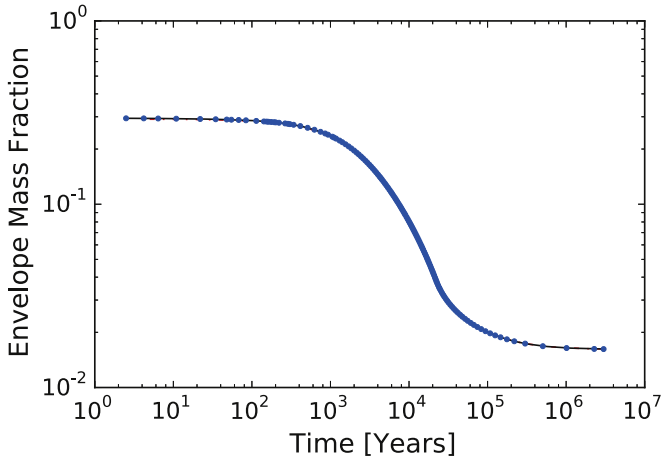

Figure 14. Evolution of the envelope mass fraction for the model with a 5 $M_\oplus$ core and initial envelope mass fraction of 30% at an equilibrium temperature of 900 K. The different lines show cases where the envelope mass fraction from which material can be removed as mass-loss is varied: <0.5% (black-solid), <1% (blue-points), <2% (red-dashed), the evolution is identical in all cases where the final envelope mass fractions at the end of the simulation are within <0.03%. Therefore, we are confident the specific range of atmosphere mass over which we remove material is not driving our results.

evolution of the envelope mass fraction for the model with a $5M_\oplus$ core and initial envelope mass fraction of 30% where the envelope mass fraction material is removed from is <0.5% (solid), <1% (points), <2% (dashed) is shown. The final envelope mass fractions at the end of the simulation are within <0.03%.

In our simulations we use a very simple technique to include the irradiation from the central star in the upper layers (but below the photosphere) of the planet's atmosphere. Where we heat a fixed column density of the atmosphere at the rate prescribed by stellar heating, the $F_* - \Sigma$ approach (Paxton et al. 2013). We chose to heat a column of 250 g cm^{-2} in all our above calculations, motivated by the opacity of 4×10^{-3} suggested by (Guillot 2010). We can check how sensitive our results are to this choice of column density by repeating the

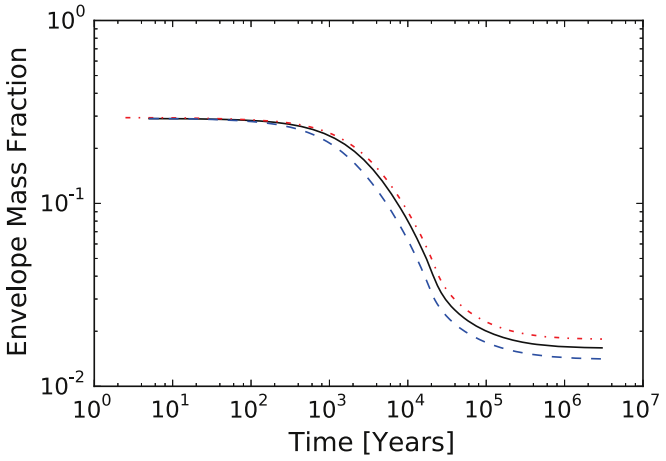

Figure 15. Evolution of the envelope mass fraction for the model with a 5 $M_\oplus$ core and initial envelope mass fraction of 30% at an equilibrium temperature of 900 K. The lines correspond to different column densities that are heated by the stellar irradiation and the values shown are: 50 (dashed), 250 (solid—the standard value used in our calculations) and 1250 (dotted–dashed) g cm^{-2}.

calculation for a model with a 5 $M_\oplus$ core and initial envelope mass fraction of 30%. We choose to heat a column density of 50 and 1250 g cm^{-2} at the surface of the atmosphere, corresponding to a factor of five change up and down of the atmospheric opacity. The results of this experiment are shown in Figure 15. As expected the results are obviously sensitive to the depth of the heating (as it in turn changes the radius of the planet), the effect of the column density heated by the stellar irradiation is a secondary effect, and all models follow a similar evolution.

Considering all the tests above we are happy that our model simplifications are not driving our results, which are robust.

REFERENCES

Alexander, R. D., Clarke, C. J., & Pringle, J. E. 2006, MNRAS, 369, 229
Arras, P., & Bildsten, L. 2006, ApJ, 650, 394
Batalha, N. M., Borucki, W. J., Bryson, S. T., et al. 2011, ApJ, 729, 27
Batalha, N. M., Rowe, J. F., Bryson, S. T., et al. 2013, ApJS, 204, 24
Bodenheimer, P., & Lissauer, J. J. 2014, ApJ, 791, 103
Borucki, W. J., Koch, D. G., Basri, G., et al. 2011, ApJ, 736, 19
Burrows, A., Guillot, T., Hubbard, W. B., et al. 2000, ApJL, 534, L97
Carter, J. A., Agol, E., Chaplin, W. J., et al. 2012, Sci, 337, 556
Chiang, E., & Laughlin, G. 2013, MNRAS, 431, 3444
Clarke, C. J., Gendrin, A., & Sotomayor, M. 2001, MNRAS, 328, 485
Cranmer, S. R. 2004, AmJPh, 72, 1397
Crida, A., Morbidelli, A., & Masset, F. 2006, Icar, 181, 587
Dressing, C. D., Charbonneau, D., Dumusque, X., et al. 2015, ApJ, 800, 135
Dumusque, X., Bonomo, A. S., Haywood, R. D., et al. 2014, ApJ, 789, 154
Ercolano, B., Clarke, C. J., & Hall, A. C. 2011, MNRAS, 410, 671
Foreman-Mackey, D., Hogg, D. W., & Morton, T. D. 2014, ApJ, 795, 64
Fortney, J. J., Marley, M. S., & Barnes, J. W. 2007, ApJ, 659, 1661
Fressin, F., Torres, G., Charbonneau, D., et al. 2013, ApJ, 766, 81
Fung, J., Artymowicz, P., & Wu, Y. 2015, arXiv:1505.03152
Gorti, U., Dullemond, C. P., & Hollenbach, D. 2009, ApJ, 705, 1237
Guillot, T. 2010, A&A, 520, A27
Guillot, T., Burrows, A., Hubbard, W. B., Lunine, J. I., & Saumon, D. 1996, ApJL, 459, L35
Hadden, S., & Lithwick, Y. 2014, ApJ, 787, 80
Haisch, K. E., Lada, E. A., & Lada, C. J. 2001, ApJL, 553, L153
Hansen, B. M. S., & Murray, N. 2012, ApJ, 751, 158
Hatzes, A. P., Fridlund, M., Nachmani, G., et al. 2011, ApJ, 743, 75
Hernandez, J., Calvet, N., Briceno, C., et al. 2007, ApJ, 671, 1784
Ida, S., & Lin, D. N. C. 2005, ApJ, 626, 1045
Ida, S., & Lin, D. N. C. 2010, ApJ, 719, 810
Ikoma, M., & Hori, Y. 2012, ApJ, 753, 66

Jontof-Hutter, D., Lissauer, J. J., Rowe, J. F., & Fabrycky, D. C. 2014, ApJ, 785, 15
Kenyon, S. J., & Hartmann, L. 1995, ApJS, 101, 117
Koepferl, C. M., Ercolano, B., Dale, J., et al. 2013, MNRAS, 428, 3327
Lee, E. J., & Chiang, E. 2014, arXiv:1510.08855
Lee, E. J., Chiang, E., & Ormel, C. W. 2014, ApJ, 797, 95
Lissauer, J. J., Fabrycky, D. C., Ford, E. B., et al. 2011, Natur, 470, 53
Lissauer, J. J., Hubickyj, O., D'Angelo, G., & Bodenheimer, P. 2009, Icar, 199, 338
Lopez, E. D., & Fortney, J. J. 2013, ApJ, 776, 2
Mahajan, N., & Wu, Y. 2014, ApJ, 795, 32
Mamajek, E. E. 2009, in AIP Conf. Proc. 1158, Exoplanets and Disks: Their Formation and Diversity, ed. T. Usada, M. Tamura, & M. Ishii (Melville, NY: AIP), 3
Marcy, G. W., Isaacson, H., Howard, A. W., et al. 2014, ApJS, 210, 20
Masuda, K. 2014, ApJ, 783, 53
Mizuno, H., Nakazawa, K., & Hayashi, C. 1978, PThPh, 60, 699
Mullally, F., Coughlin, J. L., Thompson, S. E., et al. 2015, ApJS, 217, 31
Ofir, A., Dreizler, S., Zechmeister, M., & Husser, T.-O. 2014, A&A, 561, A103
Ormel, C. W., Shi, J.-M., & Kuiper, R. 2015, MNRAS, 447, 3512
Owen, J. E., Ercolano, B., & Clarke, C. J. 2011, MNRAS, 412, 13
Owen, J. E., Ercolano, B., Clarke, C. J., & Alexander, R. D. 2010, MNRAS, 401, 1415
Owen, J. E., & Jackson, A. P. 2012, MNRAS, 425, 2931
Owen, J. E., & Wu, Y. 2013, ApJ, 775, 105
Parker, E. N. 1958, ApJ, 128, 664
Paxton, B., Bildsten, L., Dotter, A., et al. 2011, ApJS, 192, 3
Paxton, B., Cantiello, M., Arras, P., et al. 2013, ApJS, 208, 4
Petigura, E. A., Marcy, G. W., & Howard, A. W. 2013, ApJ, 770, 69
Piso, A.-M. A., Youdin, A. N., & Murray-Clay, R. A. 2014, ApJ, 786, 21
Pollack, J. B., Hubickyj, O., Bodenheimer, P., et al. 1996, Icar, 124, 62
Pu, B., & Wu, Y. 2015, arXiv:1502.05449
Rafikov, R. R. 2006, ApJ, 648, 666
Raymond, S. N., & Cossou, C. 2014, MNRAS Lett., 440, L11
Rogers, L. A. 2014, arXiv:1407.4457
Rogers, L. A., & Seager, S. 2010, ApJ, 712, 974
Silburt, A., Gaidos, E., & Wu, Y. 2015, ApJ, 799, 180
Weiss, L. M., & Marcy, G. W. 2014, ApJL, 783, L6
Wolfgang, A., & Lopez, E. 2015, ApJ, 806, 183
Wolfgang, A., Rogers, L. A., & Ford, E. B. 2015, arXiv:1504.07557
Wood, B. E., Muller, H., Zank, G. P., & Linsky, J. L. 2002, ApJ, 574, 412
Wu, Y., & Lithwick, Y. 2013, ApJ, 772, 74